This article has been accepted for inclusion in a future issue of this journal. Content is final as presented, with the exception of pagination.

Effect of Threading Dislocations on GaInP Front- and Rear-Junction Solar Cells Grown on Si

Brian Li, Pankul Dhingra, Ryan D. Hool, Shizhao Fan, and Minjoo Larry Lee, *Senior Member, IEEE*

***Abstract*—We compare the performance of front-junction (FJ) and rear-heterojunction (RHJ) 1.9 eV GaInP solar cells grown on Si by molecular beam epitaxy. First, time-resolved photoluminescence showed a minority carrier lifetime of 11.7 ns for *n*-GaInP on Si, indicating a high tolerance to threading dislocations due to the low mobility of minority holes. GaInP solar cells were grown on both GaAs and Si substrates in FJ (*p*-type absorber) and RHJ (*n*-type absorber) configurations. The internal quantum efficiency (IQE) of FJ cells was identical on GaAs and Si substrates and showed high IQE-derived short-circuit current density $J_{SC,IQE} > 14$ mA/cm^2, suitable for high-efficiency multijunction cells, while RHJ cells showed diminished $J_{SC,IQE} < 11$ mA/cm^2 due to limited diffusion length and high sensitivity to front-surface recombination. The RHJ cells on Si maintained a high open-circuit voltage (V_{OC}) of 1.292 V with threading dislocation density (TDD) of 1.0×10^7 cm^{-2}, a similar V_{OC} value to FJ cells grown lattice-matched on GaAs. In addition, for a high TDD of 2.7×10^8 cm^{-2}, RHJ cells had a V_{OC} of 1.223 V, greater than FJs with 10× lower TDD of 2.7×10^7 cm^{-2}, which further shows the high dislocation tolerance of n-GaInP. The high V_{OC}, combined with the proposed work to boost IQE, could enable GaInP RHJs on Si for multijunction cell applications.**

***Index Terms*—GaInP, III-V on Si, metamorphic, molecular beam epitaxy (MBE).**

I. Introduction

Single-junction (1J) Si solar cells, by far the most dominant photovoltaic technology, are approaching their fundamental efficiency limit of 29.4% [1] at both the laboratory and commercial scale [2]. Multijunction solar cells (MJSCs) using a Si bottom cell have theoretical efficiencies of 37%–44% [3], [4] for 2- and 3-junctions, respectively, and are a promising approach to reduce cost per watt. III–V on Si MJSCs use a variety of integration approaches, such as wafer bonding, mechanical stacking, and direct growth. Both wafer bonding and mechanical stacking have achieved record III-V/Si MJSC efficiencies of 35.9% [5], [6], well beyond the Si single-junction efficiency limit. In contrast, while the efficiency of epitaxial III–V/Si cells has increased significantly in recent years [7], [8], [9], the record efficiency of 25.9% [9] is well below bonded and mechanically stacked cells due to nonradiative recombination at threading dislocations. Despite the lower efficiency, a key advantage of direct growth is its simpler fabrication process, which could enable greater scalability.

Yamaguchi's model of the effect of dislocations on minority carrier lifetime τ is given as [10]

$$\frac{1}{\tau} = \frac{1}{\tau_0} + \frac{1}{\tau_{TDD}} \tag{1}$$

where τ_0 is the nominal lifetime for dislocation-free material, while τ_{TDD} is the nonradiative lifetime due to dislocations. In this equation, τ_{TDD} is further defined as

$$\tau_{TDD} = \frac{4}{\pi^3 \; D \; \mathrm{TDD}} \tag{2}$$

where D is the minority carrier diffusivity and TDD is the threading dislocation density. Since electrons have ∼10–20× higher diffusivity than holes in most direct-gap III-V absorber materials, cells with a primarily *p*-type absorber (relying on the collection of minority electrons) are more sensitive to TDD than those with a primarily *n*-type absorber (relying on collection of minority holes). In p-GaAs, lifetime degrades more rapidly than in *n*-GaAs as a function of TDD [11], and, accordingly, open-circuit voltage (V_{OC}) of n^+/p GaAs solar cells degrade more strongly with increasing TDD than p^+/n cells at a given TDD [12]. Nevertheless, the high diffusivity of minority electrons in *p*-GaAs can enable reasonable diffusion length and carrier collection of minority electrons in the presence of dislocations, as exemplified by the high J_{SC} of 26.5 mA/cm^2 for n^+/p front-junction (FJ) GaAs cells on Si with TDD of 7×10^6 cm^{-2} [13].

GaInP cells show greater experimental dislocation tolerance than GaAs in external quantum efficiency (EQE) and open-circuit voltage (V_{OC}) [7], [8], [14]. The EQE-derived short-circuit current density of epitaxial GaInP cells on Si ranges from 12.2 to 13.0 mA/cm^2, with more recently reported cells thinned to 390–400 nm to improve current matching to the underlying GaAs subcell [8], [9]. In addition, subcell GaInP V_{OC} extracted from electroluminescence (EL) showed V_{OC} loss on Si exceeding 100 mV for TDD in the range of 2.2×10^7–1.4×10^8 cm^{-2}

Manuscript received 30 November 2023; revised 4 March 2024; accepted 29 March 2024. The work of Brian Li and Ryan D. Hool was supported by NASA Space Technology Research Fellowships under Grant 80NSSC19K1174 and Grant 80NSSC18K1171. The work of Pankul Dhingra was supported by DOE SETO Grant # DE-EE0008545. The work of Shizhao Fan and Minjoo Lee was supported by the National Science Foundation under Grant 1736181 and Grant 1719567. *(Corresponding author: Minjoo Larry Lee.)*

Brian Li, Pankul Dhingra, and Minjoo Larry Lee are with the University of Illinois Urbana-Champaign, Champaign, IL 61820 USA (e-mail: bdli2@illinois.edu; pankuld2@illinois.edu; mllee@illinois.edu).

Ryan D. Hool is with the University of Illinois Urbana-Champaign, Champaign, IL 61820 USA, and also with SolAero by Rocket Lab, Albuquerque, NM 87123 USA (e-mail: rhool@illinois.edu).

Shizhao Fan is with the University of Illinois Urbana-Champaign, Champaign, IL 61820 USA, and also with the Suzhou Institute of Nano-Tech and Nano-Bionics, Chinese Academy of Sciences, Jiangsu 215123, China (e-mail: szfan2020@sinano.ac.cn).

Color versions of one or more figures in this article are available at https://doi.org/10.1109/JPHOTOV.2024.3385730.

Digital Object Identifier 10.1109/JPHOTOV.2024.3385730

© 2024 The Authors. This work is licensed under a Creative Commons Attribution-NonCommercial-NoDerivatives 4.0 License. For more information, see https://creativecommons.org/licenses/by-nc-nd/4.0/

This article has been accepted for inclusion in a future issue of this journal. Content is final as presented, with the exception of pagination.

(a)	(b)
100 nm n-AlInP barrier, n = 1×10^{18} cm^{-3}	100 nm p-AlGaInP barrier, p = 1×10^{18} cm^{-3}
500 nm n-GaInP absorber, n = 1×10^{17} cm^{-3}	500 nm p-GaInP absorber, p = 1×10^{17} cm^{-3}
100 nm n-AlInP barrier, n = 1×10^{18} cm^{-3}	100 nm p-AlGaInP barrier, p = 1×10^{18} cm^{-3}
100 nm n^{+}-GaAs buffer	100 nm p^{+}-GaAs buffer
500 nm UID-GaAs buffer	500 nm UID-GaAs buffer
SI-GaAs or GaAs/Si (001)	**SI-GaAs or GaAs/Si (001)**

Fig. 1. Layer structures for (a) *n*-GaInP and (b) *p*-GaInP DHs grown on semi-insulating (SI) GaAs and on GaAs/Si (001).

Layer	Material	Doping	Thickness
Sputtered SiO_2			
Sputtered TiO_2			
Contact	n^{+}-GaAs		
Window	n-AlInP	1x10^{18} cm^{-3}	20 nm
Emitter	n-GaInP	2x10^{18} cm^{-3}	50 nm
Base	p-GaInP	1x10^{17} cm^{-3}	710 nm
BSF	p-GaInP	2x10^{18} cm^{-3}	50 nm
BSF	p-AlInP	2x10^{18} cm^{-3}	50 nm
Contact	p^{+}-GaAs	7x10^{18} cm^{-3}	150 nm
p-GaAs or GaAs/Si (001)			

(a)

Layer	Material	Doping	Thickness
Contact	n^{+}-GaAs		
Window	n-AlInP	1x10^{18} cm^{-3} (w/ δ spikes)	20 nm
Emitter	n-GaInP	1x10^{17} cm^{-3}	810 nm or 500 nm
BSF	p-AlGaInP	1x10^{17} cm^{-3}	100 nm
Buffer	p-AlGaAs	2.4x10^{18} cm^{-3}	100 nm
Contact	p^{+}-GaAs	7x10^{18} cm^{-3}	500 nm
p-GaAs or GaAs/Si (001)			

(b)

Fig. 2. Growth structures for (a) FJ and (b) RHJ GaInP cells grown on *p*-GaAs and GaAs/Si (001).

[7], [8] compared to >200 mV loss for GaAs on Si. However, relative to GaAs, there have been limited studies to quantify GaInP on Si cell performance as a function of TDD or cell design [15], [16]. A detailed study of GaInP cells versus TDD would greatly inform the optimal design for III–V on Si MJSCs.

The standard GaInP cell design is the FJ n^{+}/p or p^{+}/n cell, which consists of a thin n^{+}- or p^{+}-emitter on a thick *p*- or *n*-type base to maximize photocarrier generation and collection near the space charge region (SCR). However, to date, the highest efficiency GaInP cells lattice-matched on GaAs have used a rear-heterojunction (RHJ) *n*-on-*p* design, in which a thick (>800 nm), lightly doped (1–5 $\times$ 10^{17} cm^{-3}) *n*-type GaInP absorber forms a junction on top of *p*-AlGaInP [17], [18], [19]. Due to their junction placement far from the highest photocarrier region, RHJ cells require high minority carrier diffusion length to achieve similar EQE to FJs, and may be particularly sensitive to defects that lower diffusion length. As an example, rear-junction $GaAs_{0.75}P_{0.25}$ 1J cells on GaAs showed improved V_{OC} over FJ cells but also lower QE due to the higher sensitivity of the rear-junction cell to diffusion length [20]. However, since minority hole mobilities in GaInP are several times lower than in GaAs or GaAsP, the V_{OC} and QE of GaInP rear-junction cells may be more resilient to dislocations [15], motivating a comparative study of FJ and RHJ GaInP cells on Si.

In this work, we first report lifetime studies with time-resolved photoluminescence (TRPL) on *n*-GaInP and *p*-GaInP double heterostructures (DHs) grown on both GaAs and Si, obtaining a peak *n*-GaInP lifetime on Si of 11.7 ns. Next, the performance of GaInP FJ and RHJ cells on GaAs and Si were compared. FJ cells had superior carrier collection on both substrates due to superior junction placement, while RHJs had superior V_{OC} and minimal V_{OC} degradation on Si due to the use of the *n*-type absorber. Finally, we propose paths to boost the carrier collection of RHJs to leverage their superior absorber material quality.

II. Methods

All DHs and solar cells were grown by solid-source molecular beam epitaxy (MBE) using a Veeco Mod Gen II MBE system. The dopants used were Si for *n*-type layers and Be for *p*-type layers. GaAs was grown on GaP/Si (001) from $NAsP_{III-V}$ GmbH to form GaAs/Si templates, and samples were subsequently cogrown on GaAs substrates and GaAs/Si. GaInP layers were grown at a substrate temperature of 460 °C and a growth rate of 0.5 μm/h. The *n*-type and *p*-type GaInP DHs, given in Fig. 1, had a 500-nm GaInP absorber layer with doping of 1 $\times$ 10^{17} cm^{-3}, the same doping as the main absorber regions for the RHJ and FJ cells. The *n*-GaInP and *p*-GaInP DHs used 2.3 eV *n*-$Al_{0.52}In_{0.48}P$ (hereafter AlInP) and 2.2 eV *p*-$Al_{0.24}Ga_{0.28}In_{0.48}P$ (hereafter AlGaInP) for the barrier layers to match the window and back-surface field (BSF) passivating layers, respectively, in the solar cells.

The layer structures for GaInP FJ and RHJ solar cells are given in Fig. 2. The growth structure of the GaAs/Si template varied for the cells and DHs: for the FJs, we grew a 3.64 μm $GaAs_{y}P_{1-y}$ step-graded buffer prior to GaAs growth, while for the RHJs and DHs, we utilized a GaAs/Si template design consisting of 1.8–2.6 μm GaAs buffer layers with inserted InGaAs dislocation filter layers and thermal cycle annealing to reduce TDD [21], [22]. However, while buffer designs differed, the primary interest

This article has been accepted for inclusion in a future issue of this journal. Content is final as presented, with the exception of pagination.

in this work is cell performance as a function of TDD rather than of specific buffer design. From top to bottom, the FJ cells consisted of a 20 nm AlInP window ($n = 1 \times 10^{18}$ cm^{-3}), a 50 nm n-GaInP emitter ($n = 2 \times 10^{18}$ cm^{-3}), a 710 nm p-GaInP base ($p = 1 \times 10^{17}$ cm^{-3}), and finally both a 50 nm p-GaInP BSF ($p = 2 \times 10^{18}$ cm^{-3}) and AlInP BSF ($p = 2 \times 10^{18}$ cm^{-3}) for rear surface passivation. The RHJ cells consisted of a 20 nm n-AlInP window ($n = 5 \times 10^{18}$ cm^{-3}), a 500-810 nm n-GaInP emitter ($n = 1 \times 10^{17}$ cm^{-3}), and a 100 nm p-AlGaInP BSF ($p = 1 \times 10^{17}$ cm^{-3}), with the junction at the emitter/BSF interface. The RHJ AlInP window had 5× higher doping than FJs to improve front-surface passivation, which was vital for high-performance GaInP RHJs [19], and this higher doping was achieved by the addition of four delta-doped layers of Si (0.01 monolayers each). Compared to the n-AlInP barriers for the n-GaInP DH, the n-AlInP window on the RHJs is much thinner, so higher doping was needed to provide a comparable level of surface passivation.

A two-layer antireflection coating (ARC) of TiO_x/SiO_x was sputtered onto the FJs, while no ARC was applied to the RHJs. We performed postgrowth rapid thermal annealing (RTA) to improve the phosphide material quality of both DHs and cells, as reported previously [19], with temperatures of 750–1000 °C and annealing times of 10–120 s. Cells were processed using standard lithography and metal deposition techniques, with device dimensions of 1.1 mm × 1.1 mm; metal contacts were deposited on the top surfaces of the n^+-GaAs and p^+-GaAs contact layers shown in Fig. 2. To measure TDD, we used cathodoluminescence (CL) for DHs and electron beam-induced current (EBIC) mapping for processed solar cell devices.

DH lifetimes were measured by TRPL using a pulsed super-continuum laser under low-level injection conditions (<5×10^{15} cm^{-3} carriers) with a single photon detection module (ID Quantique, model No. id 100-20). For this setup, measurements for accurate TRPL lifetimes (τ_{TRPL}) were limited to $\tau_{\text{TRPL}} > 1.3$ ns due to overlap with the system response function. For solar cells, lighted current-voltage (LIV) measurements were obtained under approximate AM1.5G conditions using an ABET 10 500 solar simulator. EQE and reflectance were measured with a PV Measurements QEX7 system to obtain internal quantum efficiency (IQE) by the equation IQE = EQE/(1-R). Finally, we extract the dark current parameters J_{01} and J_{02} from Suns-V_{oc} and dark current-voltage measurements.

III. Results and Discussion

The τ_{TRPL} value of the n-GaInP DH was much higher than p-GaInP for growth on both GaAs and GaAs/Si, as shown in Fig. 3(a). The TDD for the DH structures ranged from 8.0–9.4 × 10^6 cm^{-2}, with a representative CL image for the n-GaInP DH in Fig. 4(a). Remarkably, the n-GaInP DH grown on GaAs/Si experiences only a modest degradation in τ_{TRPL} from 14.6 to 11.7 ns. The mechanisms of higher nonradiative recombination in p-GaInP DHs are uncertain; a ∼10× higher surface recombination velocity (SRV) has been measured for p-GaInP DHs compared to n-GaInP DHs [23], but bulk lifetime is still several times lower after accounting for SRV. τ_{TRPL} of

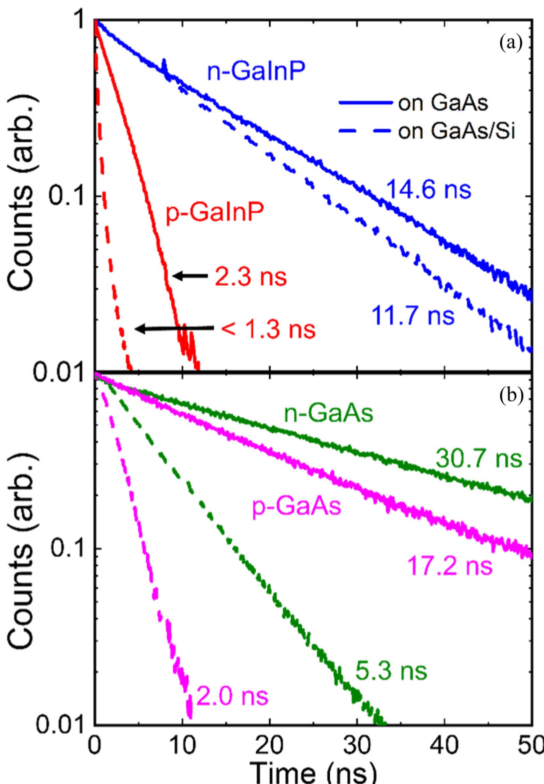

Fig. 3. TRPL decay curves on GaAs substrates (solid) and GaAs/Si templates (dashed) for (a) GaInP DHs and (b) GaAs DHs. The n-GaInP DH shows minimal lifetime degradation on GaAs/Si.

the p-GaInP DH decreased from 2.3 ns on GaAs to < 1.3 ns on GaAs/Si; τ_{TRPL} of the p-GaInP DH on GaAs/Si was too low to be accurately measured with the setup due to overlap with the system response function. For comparison purposes, we also grew n- and p-GaAs DHs on GaAs and GaAs/Si with the same thickness, doping, and TDD as the GaInP DHs. τ_{TRPL} of the n-GaAs DH degraded from 30.7 to 5.3 ns for growth on GaAs/Si (5.7× decrease), while the lifetime of the p-GaAs DH degraded from 17.2 to 2 ns (8.6× decrease) for growth on GaAs/Si. The minority carrier diffusivity in n-GaInP (∼2 cm^2/s) is much lower than that in n-GaAs and p-GaAs (∼8 and 80 cm^2/s, respectively), leading to its higher dislocation tolerance.

Next, a pair of RHJ solar cells were cogrown on GaAs (RHJ1) and GaAs/Si at a TDD of 1.0 × 10^7 cm^{-2} (RHJ2) with n-GaInP emitter thickness of 810 nm, while a third RHJ was separately grown on GaAs/Si at a high TDD of 2.7 × 10^8 cm^{-2} (RHJ3), with emitter thickness of 500 nm. For FJs, two cells were cogrown on GaAs (FJ1) and GaAs/Si at TDD of 2.7 × 10^7 cm^{-2} (FJ2). Fig. 4(b)–(d) shows representative EBIC images for all three cells grown on GaAs/Si; each black dot is a threading dislocation, and the absence of black lines indicates there are no misfit dislocations in the active region of the cells.

The IQE spectra of FJ cells were insensitive to TDD, with virtually identical spectra (see Fig. 5) and IQE-derived J_{SC} values $J_{\text{SC,IQE}} > 14.0$ mA/cm^2 under the AM1.5G spectrum (see Table I), on par with those reported in prior epitaxial tandems on Si [6], [7], [9], [14]. In contrast, the best $J_{\text{SC,IQE}}$ for the RHJs

This article has been accepted for inclusion in a future issue of this journal. Content is final as presented, with the exception of pagination.

TABLE I
DESCRIPTION AND FIGURES OF MERIT FOR GAINP SOLAR CELLS IN THIS WORK

FJ (w/ ARC)	TDD (cm^{-2})	GaInP thickness (nm)	Peak IQE (%)	IQE-derived J_{SC} (mA/cm^2)	V_{OC} (V)	J_{SC} (mA/cm^2)	FF (%)	η (%)	J_{02} (A/cm^2)
FJ1	$<5.0 \times 10^3$	810	91.9	14.0	1.299	12.9	78.1	13.1	2.1×10^{-13}
FJ2	2.7×10^7	810	92.8	14.3	1.216	13.4	74.8	12.2	8.0×10^{-13}
RHJ (no ARC)									
RHJ1	$<5.0 \times 10^3$	810	57.8	9.3	1.333	6.2	79.5	6.5	2.4×10^{-14}
RHJ2	1.0×10^7	810	65.9	10.8	1.292	7.4	78.3	7.4	1.0×10^{-13}
RHJ3	2.7×10^8	500	38.3	5.8	1.223	4.0	73.0	3.5	1.9×10^{-13}

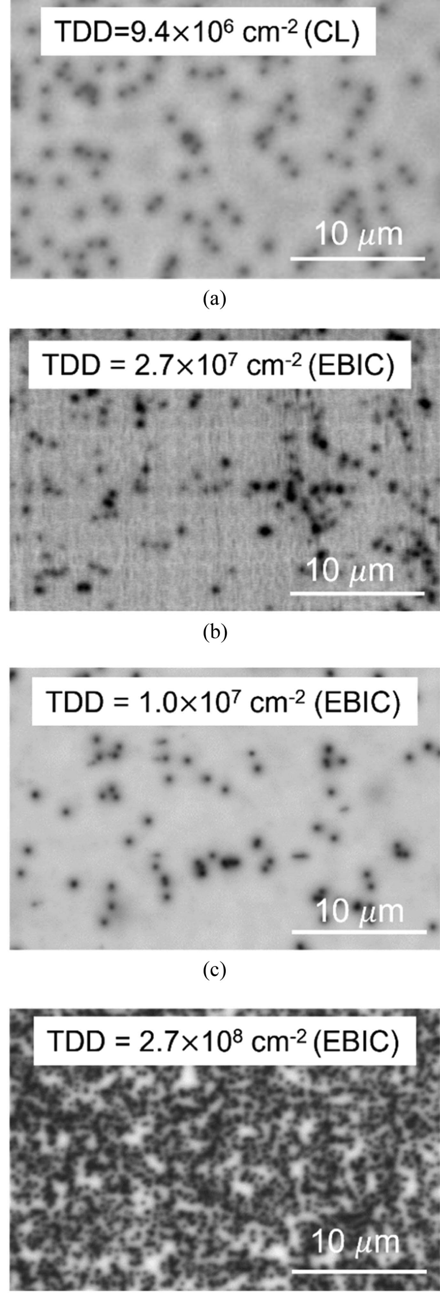

Fig. 4. (a) Representative CL image of n-GaInP DH on Si and (b)–(d) representative EBIC images for FJ2, RHJ2, and RHJ3. For both CL and EBIC images, each black dot represents a thread.

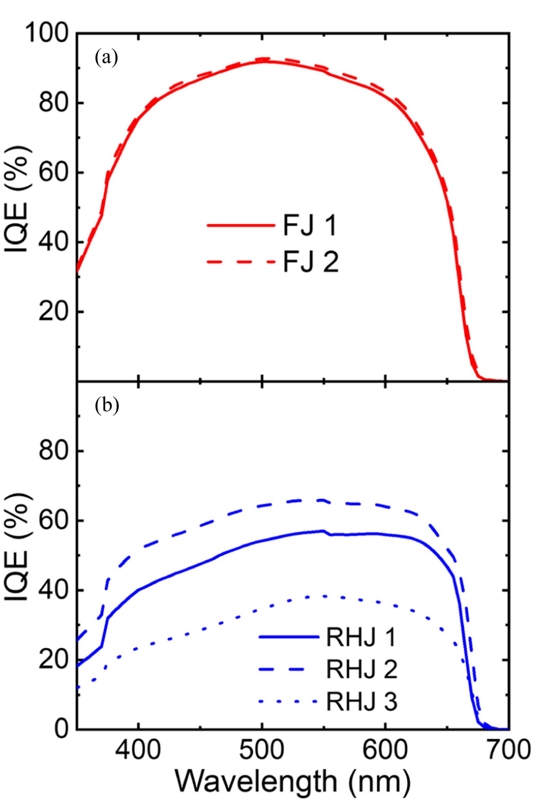

Fig. 5. IQE curves of (a) FJ and (b) RHJ cells.

was in RHJ2 with a value of only 10.8 mA/cm^2. In addition, RHJ1 had worse IQE than RHJ2 despite having superior bulk material quality as indicated by the higher V_{OC} (see Table I). The low IQE of RHJ1 on GaAs indicates contributing factors other than TDD to poor carrier collection in these cells. We believe one significant cause of the lower IQE of RHJ1 is higher front SRV, to which rear-junction cells are known to be highly sensitive [19], [20]. This theory is supported by the fact that J_{01}, which depends on both bulk quality and SRV [24], was 2.8× higher in RHJ1 than RHJ2. The window design may need further improvements beyond the additional delta-doping layers to provide reliable front-surface passivation of RHJs.

We next used Hovel modeling of IQE [25] to quantify the performance limitation in the RHJs and optimize the absorber thickness. From modeling, the FJ base and RHJ emitter of the moderate TDD cells (FJ2 and RHJ2) had comparable minority

This article has been accepted for inclusion in a future issue of this journal. Content is final as presented, with the exception of pagination.

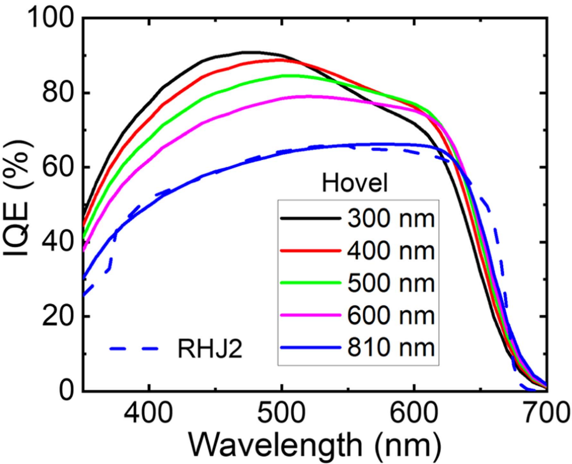

Fig. 6. Hovel IQE of RHJ design (solid) as a function of emitter thickness using fitted diffusion length of 700 nm from RHJ2 (dotted line).

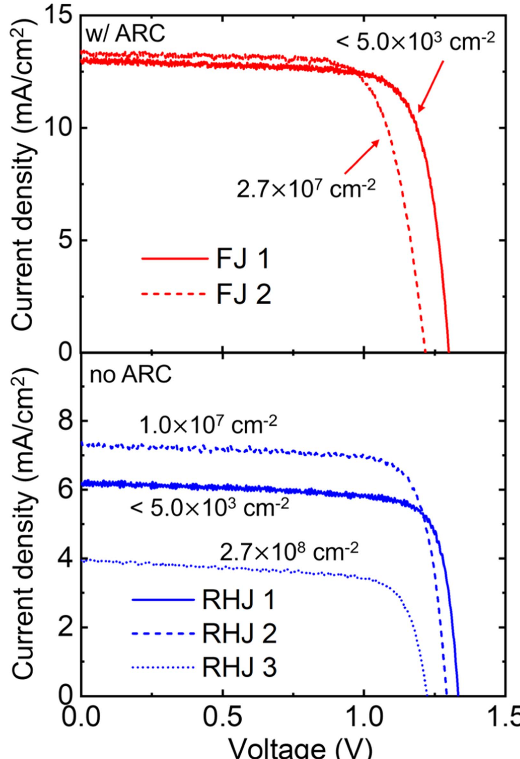

Fig. 7. LIV curves of FJ cells (w/ ARC) and RHJ cells (no ARC).

carrier diffusion lengths $L_{n,p}$ of $\sim$700 nm. The similar diffusion length is evidence of greater carrier lifetime in the RHJ emitter, given the much lower minority hole mobility. However, the junction placement far from the top surface, where most carrier generation occurs, resulted in worse IQE at similar $L_{n,p}$. Next, modeling IQE as a function of RHJ emitter thickness (see Fig. 6), $J_{\rm SC,IQE}$ was optimized at an emitter thickness of 400 nm, with a value of 13.4 mA/cm^2 that approaches the FJ value as well as $J_{\rm SC}$ values in literature.

The RHJ cells also had lower efficiency from LIV measurements (see Table I and Fig. 7) due to the low $J_{\rm SC}$ of the RHJs, which stems from both the lack of ARC and diminished IQE. However, the RHJ2 with a TDD of 1.0×10^7 cm^{-2} shows $V_{\rm OC} = 1.292$ V, comparable to the nearly dislocation-free FJ1 at 1.299 V. In addition, RHJ3 has a $V_{\rm OC}$ of 1.223 V, greater than the 1.216 V of FJ2 despite having 10× higher TDD and being in a regime where carrier lifetime is dominated by nonradiative recombination at threading dislocations. These high $V_{\rm OC}$ values for the RHJs are especially notable given that their low $J_{\rm sc}$ values will also lower the $V_{\rm OC}$.

$V_{\rm OC}$ comparisons for the FJ and RHJ cells are complicated by their dependence on $J_{\rm sc}$, J_{01}, and J_{02} as given by solving the double-diode model at the open-circuit condition

$$J_{sc} = J_{01}\ \exp\left(\frac{qV_{OC}}{kT}\right) + J_{02}\exp\left(\frac{qV_{OC}}{2kT}\right) \quad (3)$$

where k is the Boltzmann constant, T is the temperature, and q is the unit charge. J_{01} and J_{02} are dependent on the bulk carrier lifetime, while J_{01} is additionally affected by SRV. The effect of SRV is notable when comparing RHJ1 to RHJ2, in which the higher J_{01} of RHJ1 accounts for $\sim$26 mV of $V_{\rm OC}$ loss relative to RHJ2. However, for a more objective comparison of bulk material quality in the different solar cells as a function of TDD, we will primarily compare J_{02} values. The J_{02} dark current, which stems from recombination in the SCR, is approximated by

$$J_{02} = \frac{q\ W\ n_i}{2\tau} \quad (4)$$

where W is the depletion region width, n_i is the intrinsic carrier concentration, and τ is the minority carrier lifetime. The $V_{\rm OC}$ due to J_{02} dark current is then given by [12]

$$V_{OC} = \frac{2kT}{q}\ \ln\left(\frac{J_{SC}}{J_{02}}\right). \quad (5)$$

The experimental J_{02} values are given in the right-most column of Table I. For both FJs and RHJs, J_{02} increased by $\sim$4× when comparing the cells on GaAs (FJ1 and RHJ1) to the cells on Si at moderate TDD (FJ2 and RHJ2), with a decrease in calculated $V_{\rm OC}$ of 69.2 mV and 74.5 mV for FJs and RHJs, respectively. From RHJ2 to RHJ3, the J_{02} increases by a further 1.9×, with a decrease in $V_{\rm OC}$ of only 32 mV. The experimental J_{02} values for the cells grown on Si (FJ2, RHJ2, and RHJ3) were 8.0×10^{-13}, 1.0×10^{-13}, and 1.9×10^{-13} A/cm^2, respectively, showing much lower J_{02} values for RHJs even with a 10× higher TDD in RHJ3. The greatly reduced J_{02} of both RHJs may be due to both a smaller depletion region width and higher lifetime in the n-GaInP absorber. One assumption for the RHJs is that the contribution of the 2.2 eV AlGaInP BSF to J_{02} is minimal, since the 300 meV higher bandgap leads to almost 3 orders of magnitude lower intrinsic carrier concentration. With this assumption, the effective SCR width for the RHJ cells is approximately 109.1 nm (depletion on the GaInP emitter only), while the total SCR width of the FJ is 164.7 nm, including both the emitter and base contributions. This difference could approximately account for a 1.5× drop in the J_{02}, while the experimental J_{02} drops for RHJ2 and RHJ3 are 8× and 4.2×, respectively. Therefore, superior lifetime in the n-GaInP region

This article has been accepted for inclusion in a future issue of this journal. Content is final as presented, with the exception of pagination.

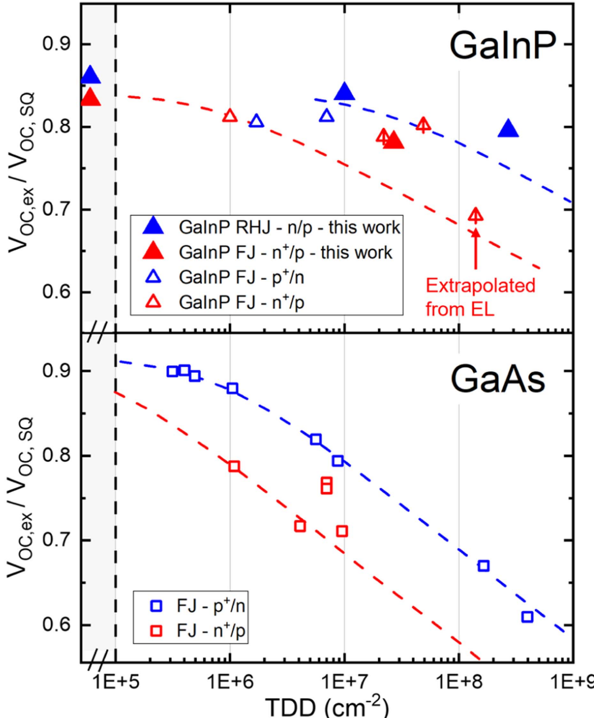

Fig. 8. V_{oc} fraction of GaInP and GaAs cells as a function of TDD. Grey bars on the left are for growth on lattice-matched GaAs substrates. GaAs cells (hollow squares) are from [12] and [13] whereas GaInP cells (hollow triangles) are from [7], [8], [16], [27] and coplotted with cells from this work (solid triangles). The hollow triangles with a bisecting vertical line were extrapolated from EL measurements assuming $n = 2$ ideality factor. Dotted lines are calculated Yamaguchi degradation curves from [16]. GaInP RHJs and p^+/n GaInP FJs showed the least degradation among the cell types.

of the RHJs should also contribute significantly to the reduced J_{02} of cells on GaAs/Si, as promised by the TRPL study. If J_{sc} of RHJ3 were boosted to similar levels as FJ2, the V_{OC} value would be ∼70 mV greater than FJ2 rather than only 7 mV higher.

The high V_{OC} retention of RHJ cells on GaAs/Si compared to FJ cells on GaAs/Si correlates well with both existing literature and prior models of V_{OC} as a function of TDD. Fig. 8 summarizes literature data for GaInP and GaAs cells on Si as a function of TDD, plotted in terms of a V_{OC} fraction $V_{OC,ex}/V_{OC,SQ}$ where $V_{OC,ex}$ is the experimental V_{OC} value and $V_{OC,SQ}$ is the Shockley-Queisser value under AM1.5G spectrum [26]. $V_{OC,SQ}$ was adjusted for each GaInP device according to their E_g values, which ranged from 1.83–1.90 eV. Several of the GaInP n^+/p FJ data points were extrapolated from EL subcell measurements of GaInP from a many-suns intensity down to the 1-sun condition (hollow triangles with vertical line) [7], [8]. The extrapolated 1-sun V_{OC} values assume an $n = 2$ ideality factor, which should dominate with high TDD [12]. Finally, the modeled V_{OC} versus TDD degradation curves (dotted lines) from Andre [16] used Yamaguchi's lifetime model for V_{OC} degradation for both n^+/p and p^+/n polarities of GaInP and GaAs FJ solar cells. Given the wide variability in experimental lattice-matched solar cell performance, comparisons between the cells are most apt at larger TDD values where performance is dominated by τ_{TDD} and the minority carrier mobility of the absorber regions. From in-house Yamaguchi modeling of V_{OC} versus TDD, FJ n^+/p cells start to become dominated by threading dislocations (defined as a 10 mV loss of V_{OC}) at TDD = 1×10^7 cm^{-2}, while the p^+/n FJ and n/p RHJ cells do not become TDD-dominated until TDD = 7×10^7 cm^{-2}. In these elevated TDD ranges, Fig. 8 illustrates the resilience of the RHJ cells in this work compared to FJ cells. In addition, the comparison between GaInP and GaAs highlights the steep drop in the V_{OC} of GaAs cells as a function of TDD. Our results clearly demonstrate the low V_{OC} degradation of RHJ GaInP cells, motivating further work, particularly on improving the IQE of RHJ cells on Si.

IV. Conclusion

In this work, FJ GaInP cells on Si showed significantly higher current collection than RHJs, with J_{SC} values comparable to the best GaInP on Si subcells in the literature, and no J_{SC} degradation from GaAs to Si substrates. However, the high dislocation tolerance of RHJ cells relative to FJ, as shown by greater V_{OC} and reduced J_{02}, even at TDD $> 1 \times 10^8$ cm^{-2}, also motivates further efforts to study RHJ cells for MJSC applications. For future work, annealing conditions on GaAs/Si with lower temperature (700–750 °C) and longer time (10–60 min) may improve phosphide quality in the cells over RTA. In addition, an optimized design with a thinner absorber of ∼400 nm, similar to GaInP cells already used for epitaxial III–V/Si in the literature, as well as more reliable front-surface passivation, should significantly increase the IQE of the RHJ cells towards FJ values, enabling RHJ cells for current matching on III–V/Si MJSCs.

Acknowledgment

This work was carried out in part in the Materials Research Laboratory Central Research Facilities, University of Illinois Urbana-Champaign and made use of shared facilities in the Nick Holonyak, Jr. Micro and Nanotechnology Laboratory, University of Illinois Urbana-Champaign.

References

[1] A. Richter, M. Hermle, and S. W. Glunz, "Reassessment of the limiting efficiency for crystalline silicon solar cells," *IEEE J. Photovolt.*, vol. 3, no. 4, pp. 1184–1191, Oct. 2013.
[2] M. A. Green et al., "Solar cell efficiency tables (version 61)," *Prog. Photovolt., Res. Appl.*, vol. 31, no. 1, pp. 3–16, 2023.
[3] J. Geisz and D. Friedman, "III – N – V semiconductors for solar photovoltaic applications," *Semicond. Sci. Technol.*, vol. 17, pp. 769–777, Jul. 2002.
[4] T. J. Grassman et al., "Spectrum-optimized Si-based III-V multijunction photovoltaics," *Proc. SPIE*, vol. 8256, 2012, Art. no. 82560R.
[5] S. Essig et al., "Raising the one-sun conversion efficiency of III-V/Si solar cells to 32.8% for two junctions and 35.9% for three junctions," *Nature Energy*, vol. 2, no. 9, pp. 1–9, Aug. 2017.
[6] P. Schygulla et al., "Two-terminal III–V//Si triple-junction solar cell with power conversion efficiency of 35.9% at AM1.5g," *Prog. Photovolt., Res. Appl.*, vol. 30, no. 8, pp. 869–879, Nov. 2021.
[7] M. Feifel et al., "Direct growth of III–V/silicon triple-junction solar cells with 19.7% efficiency," *IEEE J. Photovolt.*, vol. 8, no. 6, pp. 1590–1595, Nov. 2018.
[8] M. Feifel et al., "Direct growth of a GaInP/GaAs/Si triple-junction solar cell with 22.3% AM1.5g efficiency," *Solor RRL*, vol. 3, no. 12, Aug. 2019, Art. no. 1900313.

This article has been accepted for inclusion in a future issue of this journal. Content is final as presented, with the exception of pagination.

[9] M. Feifel et al., "Epitaxial GaInP/GaAs/Si triple-junction solar cell with 25.9% AM1.5g efficiency enabled by transparent metamorphic AlxGa1−xAsyP1−y step-graded buffer structures," *Solor RRL*, vol. 5, no. 5, Feb. 2021, Art. no. 2000763.

[10] M. Yamaguchi, C. Amano, and Y. Itoh, "Numerical analysis for high-efficiency GaAs solar cells fabricated on Si substrates," *J. Appl. Phys.*, vol. 66, no. 2, pp. 915–919, Apr. 1989.

[11] C. L. Andre et al., "Impact of dislocations on minority carrier electron and hole lifetimes in GaAs grown on metamorphic SiGe substrates," *Appl. Phys. Lett.*, vol. 84, no. 18, pp. 3447–3449, Apr. 2004.

[12] C. L. Andre et al., "Impact of dislocation densities on n^+/p and p^+/n junction GaAs diodes and solar cells on SiGe virtual substrates," *J. Appl. Phys.*, vol. 98, no. 1, pp. 014502, Jul. 2005.

[13] S. Fan et al., "16.8%-efficient n+/p GaAs solar cells on Si with high short-circuit current density," *IEEE J. Photovolt.*, vol. 9, no. 3, pp. 660–665, May 2019.

[14] F. Dimroth et al., "Comparison of direct growth and Wafer bonding for the fabrication of GaInP/GaAs dual-junction solar cells on silicon," *IEEE J. Photovolt.*, vol. 4, no. 2, pp. 620–625, Mar. 2014.

[15] N. Jain and M. K. Hudait, "Impact of threading dislocations on the design of GaAs and InGaP/GaAs solar cells on Si using finite element analysis," *IEEE J. Photovolt.*, vol. 3, no. 1, pp. 528–534, Jan. 2013.

[16] C. Andre, *III-V Semiconductors on SiGe substrates For Multi-Junction Photovoltaics*. Columbus, OH, USA: Ohio State Univ., 2004.

[17] J. F. Geisz, M. A. Steiner, I. García, S. R. Kurtz, and D. J. Friedman, "Enhanced external radiative efficiency for 20.8% efficient single-junction GaInP solar cells," *Appl. Phys. Lett.*, vol. 103, no. 4, Apr. 2013, Art. no. 041118.

[18] M. Hinojosa, I. Garcia, I. Rey-stolle, and C. Algora, "Inverted rear-heterojunction GaInP solar cells using Te memory effect," *Sol. Energy Mater. Sol. Cells*, vol. 205, Nov. 2020, Art. no. 110235.

[19] Y. Sun et al., "Improving the performance of GaInP solar cells through rapid thermal annealing and delta doping," *Sol. Energy Mater. Sol. Cells*, vol. 241, Apr. 2022, Art. no. 111725.

[20] D. L. Lepkowski et al., "Investigation of rear-emitter GaAs0.75P0.25 top cells for application to III-V/Si tandem photovoltaics," *IEEE J. Photovolt.*, vol. 9, no. 6, pp. 1644–1651, Nov. 2019.

[21] D. Jung et al., "Low threading dislocation density GaAs growth on on-axis GaP/Si (001)," *J. Appl. Phys.*, vol. 122, no. 22, Dec. 2017, Art. no. 225703.

[22] P. Dhingra et al., "Low-threshold InP quantum dot and InGaP quantum well visible lasers on silicon (001)," *Optica*, vol. 8, no. 11, pp. 1495–1500, Jul. 2021.

[23] Y. Sun, *Components of Multi-junction Solar Cells Grown By Molecular Beam Epitaxy: Tunnel Junctions and (Al)GaInP Solar Cells*. New Haven, CO, USA: Yale Univ., 2020.

[24] S. Hegedus and A. Luque, *Handbook of Photovoltaic Science and Engineering*. West Sussex, England: John Wiley and Sons, 2003.

[25] H. J. Hovel, *Semiconductors and Semimetals*. New York, NY, USA: Academic, 1975.

[26] S. Rühle, "Tabulated values of the Shockley-Queisser limit for single junction solar cells," *Solor Energy*, vol. 130, pp. 139–147, Feb. 2016.

[27] M. R. Lueck et al., "Dual junction GaInP /GaAs solar cells grown on metamorphic SiGe / Si substrates with high open circuit voltage," *IEEE Electron. Device Lett.*, vol. 27, no. 3, pp. 142–144, Mar. 2006.